

Adsorption of phenol and 2,4-dichlorophenol from wastewater: kinetic and equilibrium studies

Yuzhen Li^{a,b,*}, Ning Zhang^a

^aCollege of Environmental Science and Engineering, Taiyuan University of Technology, 79 Yingze Street, Wanbailin District, Taiyuan, 030024, China, emails: liyuzhen@tyut.edu.cn/liyuzhen123456@126.com (Y. Li)

^bChina Institute for Radiation Protection, 102 Xuefu Street, Xiaodian District, Taiyuan, 030006, China

Received 2 February 2019; Accepted 26 July 2019

ABSTRACT

The template-synthesized mesoporous carbon (TSMC) was synthesized through nano-casting approach by using sucrose as the carbon precursor, KIT-6 as the template, subsequently carbonized at the temperature of 900°C. The structures and properties of the obtained TSMC were systematically characterized by XRD, TEM and N₂ adsorption/desorption isotherm. The results demonstrate that the TSMC exhibits the worm-like morphology with high specific surface area (398.77 m²/g), large pore volume (0.078 cm³/g) and uniform pore size (3.8 nm). In addition, phenol and 2,4-dichlorophenol (2,4-DCP) were also selected as the objectives to research adsorption abilities of the TSMC. Various adsorption conditions, such as the adsorbent dosage, the solution pH, the contact time, the initial concentration and the contact temperature effects were explored using a batch technique. The results show that the removal rates of phenol and 2,4-DCP from solution for the TSMC were 84.50% and 85.57%, and the adsorption capacities of phenol and 2,4-DCP on the TSMC were 21.126 and 42.784 mg/g, respectively. Moreover, their kinetic experimental data are described by the pseudo-second-order model, and their adsorption data fit the Langmuir isotherm model well predicting a high adsorption capacity of 62.0437 and 108.6957 mg/g at 30°C, respectively. The thermodynamic study also shows that the adsorption of phenol and 2,4-DCP on TSMC were both spontaneous and endothermic. Furthermore, the π - π interaction, electrostatic repulsion, H-bonding and the hydrophobicity may play important roles in the adsorption of phenol and 2,4-DCP on the TSMC.

Keywords: Mesoporous carbon; Adsorption; Phenol; 2,4-Dichlorophenol

1. Introduction

Recently, phenols have attracted great attention due to their wide resources such as effluents from coke ovens in steel plants, petroleum refineries, petrochemical, phenolic resin, and fertilizer, pharmaceutical, chemical, dye industries, coal processing, plastics, wood products, pesticide, paint and paper industries, photochemical, explosives and leather treatments [1]. Aromatic structure and substituent atoms as its basic structure, p orbital electronics in substituent atoms

and π orbital electronics on the benzene ring form a stable conjugate system [2]. As a consequence, poorly degradable, suitably fat-soluble and highly toxic lead them to harm human health and animal life by food chain accumulation even at low concentrations. So, it is essential to remove them before discharging the wastewater into water recipients.

There are many effective techniques and materials for removing phenols from water. For instance, Wu et al. [3] applied carbon-coated sepiolite clay fibers with acid pre-treatment as low-cost adsorbents, and the removal

* Corresponding author.

fraction of phenol was 57.1%. Xu et al. [4] studied that CNT hybrid polymer to remove p-chlorophenol, and the adsorption capacity was 24.13 mg/g at the optimum experimental conditions. Some other relevant works are also shown in Table 1. To enhance the removal rates toward the phenols, mesoporous carbon materials are gradually used.

Mesoporous carbons have received considerable attention owing to their large surface area, tunable pore architecture, uniform and adjustable pore size, excellent conductivity chemical stability and mechanical stability [11]. These properties make them ideal candidates for some typical applications including adsorption [12], supercapacitors [13], catalyst supports or catalysts [14] and so on.

Over the past few years, the mesoporous carbons are usually prepared by two typical methods: the strategy from mesoporous silica hard templates and the direct synthesis from block copolymer soft templates [15]. No matter the hard template or the soft template method in the preparation, carbon precursors, templates and the preparation pathways have a great impact on the structure and pore size of mesoporous carbon materials. So the choice of an appropriate carbon source, the template and the syntheses route is the most important factor in controlling the pore and morphology of the mesoporous carbon.

Specifically, phenolic resins, sucrose, furfuryl alcohol, aromatic hydrocarbons, ethylene, acenaphthene, polyacrylonitrile (PAN) and 1,5-dihydroxynaphthalene (DHN) usually are suitable as carbon precursors [16]. Among the carbon precursors, the sucrose due to the low cost, simple and environmentally friendly has received great interest to prepare mesoporous carbon. Mesoporous silica (SBA-15, SBA-16, MCM-48, MSU-H and KIT-6), zeolites, colloidal silica particles and inorganics serve as hard templates to provide high pore volume and controlled pore size distribution [17]. In particular, mesoporous silica KIT-6 with two interwoven mesoporous subnetworks is more attractive. And so far, the nanocasting route is known as a powerful preparation pathway for mesoporous carbons. In general, the preparation of mesoporous carbons via the nanocasting strategy involves filling into the pores of the hard template with a suitable carbon precursor first, this is followed by carbonization and the final removal of the template [18]. In this way, the obtained mesoporous carbons can show the suitable pore size, which may result in excellent adsorption performance. Thus Fan et al. [19] successfully studied mesoporous carbonaceous materials with uniform pore sizes (2.6–3.8 nm) by the organic–organic self-assembly approach to remove hexachlorobenzene (992.09 $\mu\text{g/g}$). In addition, Xue et al. [20] prepared a magnetic mesoporous carbon material with the pore size (7.73 nm) via solvothermal method to rapidly extract chlorophenols from water samples. Therefore, it is necessary to determine the key factor underlying the removal of phenols by mesoporous carbon with high surface and uniform pore size structure.

Herein, the research objective of this paper was to synthesize worm-like disordered mesoporous carbon with high specific surface area and uniform pore diameter by hard template method. The obtained TSMC materials were characterized by means of XRD, TEM and N_2 adsorption/desorption isotherm. To obtain a basic understanding of adsorption ability of the mesoporous carbon toward phenols

for developing the high-performance adsorbent, we selected phenol and 2,4-DCP with different structures as the objectives. Batch adsorption experiments were systematically carried out to study effects of the TSMC dosage, the solution pH, the contact time, the initial concentration and the contact temperature. On the basis of systematically revealing the influence of different factors on adsorption performance, the adsorption mechanism is further analyzed by constructing a model to fit the adsorption effect.

2. Experimental

2.1. Materials

The KIT-6 and sucrose were obtained from Chemistry and Chemical Engineering, Bohai University. The phenol was purchased from Chemical reagent corporation (Tianjin, China). 2,4-DCP was purchased from J&K Scientific Co. Ltd. (Beijing, China). HCl, H_2SO_4 , HF (10 wt.%) and NaOH were obtained from Chemical reagent corporation (Tianjin, China). Deionized water was employed in all experiment processes. All the chemicals were of analytical grade, and were used as received without any further purification. Some properties of the phenols are summarized in Table 2 [21,22].

2.2. Preparation of the template-synthesized mesoporous carbon (TSMC)

The TSMC materials were synthesized by nanocasting route technique using a hard template, and the preparation strategy of the TSMC can be briefly described by the following process as following: generally, 2.5 g sucrose was impregnated into 2.0 g KIT-6 by nanocasting approach with 0.28 g sulfuric acid at room temperature for 24 h. Subsequently, in order to polymerize sucrose completely, the mixture was cured in 160°C for 6 h. After that, the experiment operations were repeated at the condition (1.5 g sucrose/0.16 g H_2SO_4). Then, the mixture was carbonized under a N_2 atmosphere at 900°C for 4 h with a ramp rate of 10°C/min. Finally, the carbonized product was treated with HF (10 wt.%) aqueous solution to remove the silica, washed many times with distilled water until the neutral pH, dried at 80°C for 5 h. The resulted black and powder mesoporous materials were named as TSMC.

2.3. Characterization techniques

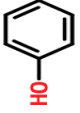
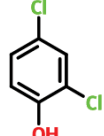
XRD patterns of the TSMC were collected by XRD-6000 diffractometer (Japan) using $\text{Cu K}\alpha$ ($\lambda = 0.15425$ nm) radiation operating at 40 kV and 30 mA with a scanning rate of 0.2°/s over the range of 0.6°–70°. The hexagonal lattice parameter (a_0) was calculated by $a_0 = 2d_{100}/\sqrt{3}$ (nm), where $d = 0.15418/(2\sin\theta)$ from Bragg's law. The microstructure of the TSMC was examined by TEM images taken by FEI F20 microscope (USA) operated at 200 kV. The sample for TEM studies was prepared by placing a drop of the suspension of the sample in ethanol onto a carbon-coated copper grid, scattered ultrasonic for 30 min at room temperature and followed by evaporating the solvent. The N_2 adsorption/desorption isotherms on the adsorbent at -196°C were determined via a Micromeritics ASAP 2020. Prior to the adsorption measurement, the sample was degassed under a vacuum at

Table 1
Comparison of the adsorption capacity for the phenols onto various materials

Adsorbent	Physical and chemical characterization	Adsorbate	Experimental conditions	Removal rates	C_0 (mg/L)	q_e (mg/g)	Reference
Bentonite-nZVI/CIMAB	S_{BET} : 2.01 m ² /g TEM: form many dendritic chains	2,4-Dichlorophenol	pH: 5.7 Material dosage: 1.0 g/L.	66.6%	48.9	–	[5]
Carbon nanotubes/porous polyimide	TEM: The PI particles are wrapped by the CNTs bundles S_{BET} : 340 m ² /g PV: 0.300 cm ³ /g	2,4-Dichlorophenol	pH: 6 Material dosage: 0.4 g/L T: 25°C	–	1,000	506	[6]
Ammonia-modified activated carbon	–	2,4-Dichlorophenol	Material dosage: 0.2 g/L Contact time: 24 h T: 30°C	–	250,	285.71	[7]
Diethylenetriamine-modified activated carbon	S_{BET} : 310 m ² /g PV: 0.14 cm ³ /g SEM: uniform morphology	Phenol	pH: 3.0–11.0 Material dosage: 2–10 g/L Contact time: 1–4 h	–	100–200	18.12	[8]
Cu-nano zeolite	S_{BET} : 890 m ² /g PV: 0.18 cm ³ /g	2-Chlorophenol	pH: 6.0 Material dosage: 4 g/L, Contact time: 2.5 h T: 20°C± 1°C	–	100	49.02	[9]
Zeolite X/activated carbon composite	S_{BET} : 872 m ² /g PV: 0.59 cm ³ /g	Phenol	pH: 6.5 T: 25°C	–	103.23	13.91	[10]
Template-synthesized mesoporous carbon	S_{BET} : 398.77 m ² /g PV: 0.078 cm ³ /g Pore size: 3.8 nm TEM: worm-like mesoporous channels	Phenol	Material dosage: 4 g/L Contact time: 2 h T: 30°C	84.50%	100	21.13	This study
Template-synthesized mesoporous carbon	S_{BET} : 398.77 m ² /g PV: 0.078 cm ³ /g Pore size: 3.8 nm TEM: worm-like mesoporous channels	2,4-Dichlorophenol	Material dosage: 4 g/L Contact time: 2 h T: 30°C	85.57%	100	42.78	This study

Notes: S_{BET} is the specific surface area, PV is the pore volume.

Table 2
Physicochemical properties of the investigated phenols

Pollutants name	Molecular weight (g/mol)	$\log K_{ow}$	Solubility (mg/L)	pKa	Structural formula
Phenol	94	1.46	93,000	9.89	
2,4-DCP	163	3.06	4,500	7.90	

80°C for 3 h to remove the guest molecules in the sample. The Brunauer–Emmett–Teller (BET) method was utilized to calculate the specific surface area of the sample from the relative pressure of $P/P_0 = 0.05–0.35$ and the average pore size distribution was derived from the desorption branch of the corresponding isotherm using the Barrett–Joyner–Halenda (BJH) method. The total pore volume was estimated from the N_2 amount adsorbed at a relative pressure of $P/P_0 = 0.99$. The elemental compositions of the sample were analyzed by vario EL element analyzer.

2.4. Adsorption performance of the TSMC

The adsorptions of phenol and 2,4-DCP on the TSMC were investigated about effects of the TSMC dosage, the solution pH, the solution concentration, the adsorption time and the adsorption temperature. Before adsorption experiments, the TSMC was kept in a desiccator. All the experiments were carried out using a 100 mL glass bottle.

In order to study the TSMC dosages, the TSMC with different mass (phenol: 0.10, 0.15, 0.20, 0.25, 0.3, 0.35, 0.40, 0.45 g and 2,4-DCP: 0.02, 0.05, 0.08, 0.10, 0.15, 0.20, 0.25, 0.30 g) were added, respectively, to the 50 mL aqueous solutions of phenol and 2,4-DCP (both the initial concentration was 100 mg/L). The mixtures were shaken in a THZ-82 shaker (Changzhou, China) at 180 rpm at 30°C for 2 h, to ensure reaching adsorption equilibrium. After adsorption, the solutions were separated from the adsorbent with a TG16-WS centrifuge (Hunan, China), and the concentrations of phenol and 2,4-DCP were measured via a UV5500-PC spectrophotometer (Shanghai, China) at the maximum wave length of 269 and 286 nm for phenol and 2,4-DCP, respectively.

The removal (%) and equilibrium q_e (mg/g) of phenol or 2,4-DCP onto TSMC at time t were calculated using the following equations:

$$\text{Removal (\%)} = \frac{C_0 - C_t}{C_0} \times 100 \quad (1)$$

where C_0 is the original concentration, while C_t (mg/L) is at time t concentration of the phenol or 2,4-DCP.

$$q_e = \frac{(C_0 - C_e) \times V}{m} \quad (2)$$

where q_e is the amount of phenols adsorbed per unit mass of adsorbent (mg/g), C_0 and C_e (mg/L) are initial and equilibrium concentration of phenols, V (L) is the volume of solution, and m (g) is the adsorbent mass.

The effect of pH was investigated in the range of 2.0–12.0 by mixing TSMC (0.2 and 0.1 g), respectively, into 50 mL phenol and 2,4-DCP solution of the initial concentration 100 mg/L for 120 min at 30°C, the pH values were adjusted by dropwise adding 0.1 mol/L NaOH or 0.1 mol/L HCl solutions.

To study the effect of adsorption time, 0.2 and 0.1 g of the TSMC were mixed with 50 mL phenol and 2,4-DCP solutions (100 mg/L) for different times separately. The effect of the solution concentration was finished at 30°C by adding 0.2 and 0.1 g of the TSMC to 50 mL phenol and 2,4-DCP solution with different initial concentrations (both 20, 40, 60, 80, 100, 120, 160, 200, 240, 280, 320, 400 mg/L) for 2 h, respectively. Through varying the temperature of the system (30°C, 35°C, 40°C), the effects of adsorption temperature on the adsorption of phenol and 2,4-DCP onto the TSMC were studied.

3. Results and discussion

3.1. Characterization of the TSMC

The structural characterization of the TSMC is inferred from XRD. As shown in Fig. 1, the low-angle XRD patterns of TSMC (see inset in Fig. 1) reveal a low-angle diffraction peaks which is not obvious at $2\theta \approx 1^\circ, 1.34^\circ, 2.10^\circ$, corresponding to the plane (211), (220), (332), suggesting a mesoporous ordering, suggesting that the ordered mesostructure is still retained after carbonization and silica removal. The reflection peaks associated with (220) and (332) become weaker, indicating that the ordered mesostructure deteriorates to some extent. The wide-angle XRD patterns show sharp diffraction peaks for the TSMC at $2\theta \approx 26.622^\circ$ ($d = 0.335$ nm) and 43.981° ($d = 0.206$ nm) which are assigned to the (002) and (100) diffractions, respectively, revealing the presence of long-range two-dimensional ordering in the carbon matrices [23]. Besides, the obvious distinctions in the full width at half maximum (FWHM) of the (002) and (100) reflection indicate the different crystallite size of the prepared TSMC [24].

To gain further insights into the morphological features, the TEM images of the TSMC were investigated. As

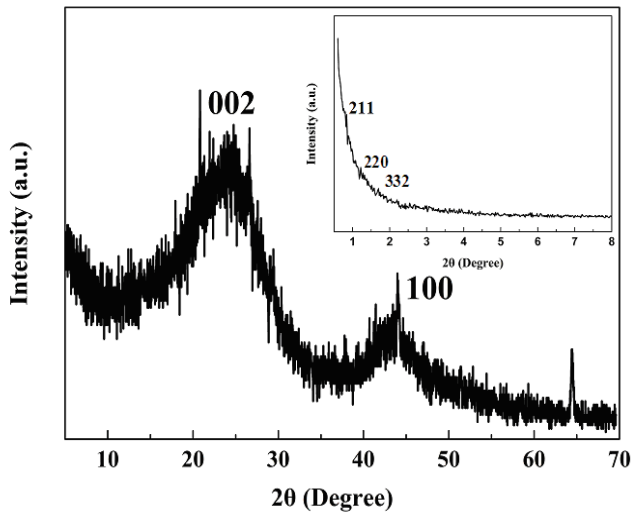


Fig. 1. Wide-angle and low-angle XRD patterns (the inset) of the TSMC.

demonstrated in Fig. 2a, the mesoporous structure consists of spherical pores that form worm-like mesoporous channels with random orientations. This phenomenon may be explained by the carbonization temperature. At low carbonization temperature, sucrose is incompletely carbonized [18]. From Fig. 2b, it can be seen that the layered structure forms the narrow slit-like pores. This means that the mesoporous preparation requires very restricted experimental conditions, especially the carbonization temperature.

The pore structure of the TSMC was evaluated by N_2 sorption analysis and the corresponding pore size distributions were inserted. As seen in Fig. 3, the TSMC shows a type-IV curve according to the IUPAC classification. At low relative pressures, the steep upwards-losing trend of the isotherm is observed, representing the presence of

microporous [25]. The pore size distribution plot of the TSMC corroborates this observation. At medium relative pressure, the TSMC shows an obvious capillary condensation supporting the existence of mesoporous [26]. At higher pressures, the N_2 adsorption smooth increasing indicates the presence of the slit-like pores, which originate from the layered structure. In addition to, from the pore size distribution curve (see inset in Fig. 3), the TSMC demonstrates narrow pore size distribution, in which the maximum peak centered at about 3.8 nm with the BJH method based on desorption branch. The TSMC has the Brunauer–Emmet–Teller (BET) surface areas of $398.77 \text{ m}^2/\text{g}$, the pore volume of $0.078 \text{ cm}^3/\text{g}$ calculated using the BJH desorption cumulative volume of pores distribution around 3.8 nm, which are all the favorable factors contributing to its excellent adsorption performance for the phenol and 2,4-DCP.

3.2. Effect of the TSMC dosage

Fig. 4 shows the removal rate (%) and the adsorption capacity of phenol and 2,4-DCP along with the TSMC dosage increasing. Specifically, from Fig. 4Aa the equilibrium removal rates of phenol rise with increase in amount of adsorbent and even reach 90.88% with 0.3 g of the TSMC. However, from Fig. 4Ab the adsorption capacity of phenol decreases from 35.07 to 15.15 mg/g with increase in amount added increase from 0.1 to 0.3 g. With a further increase in the TSMC dosage to 0.45 g, the percentage removal rates of phenol remain constant at 90.88%. The familiar situation occurs on 2,4-DCP. From Fig. 4Ba it is clear to see that the removal rates of 2,4-DCP rise rapidly from 29.25% to 85.57% with increase in amount of adsorbent from 0.02 to 0.1 g, while the equilibrium adsorption of 2,4-DCP decreases obviously from 73.12 to 42.78 mg/g with the increase in the TSMC dosage in Fig. 4Bb. And to further increase in the TSMC dosage to 0.3 g, the 2,4-DCP adsorption percentage maintain balance at 85.57%.

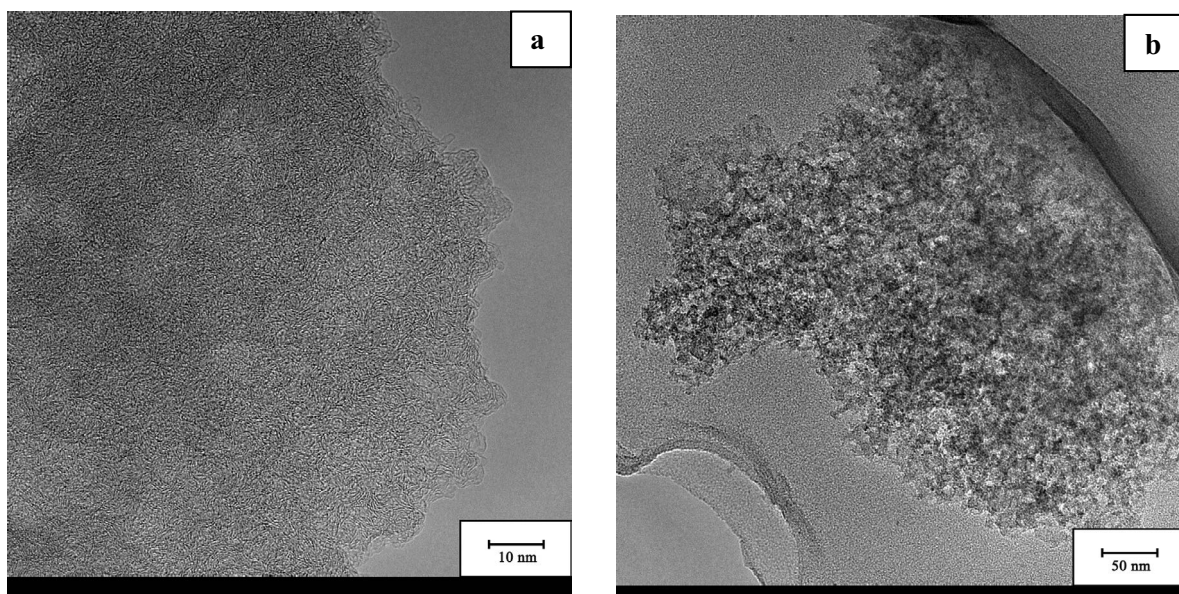


Fig. 1. TEM images of the TSMC (a) 10 nm and (b) 50 nm.

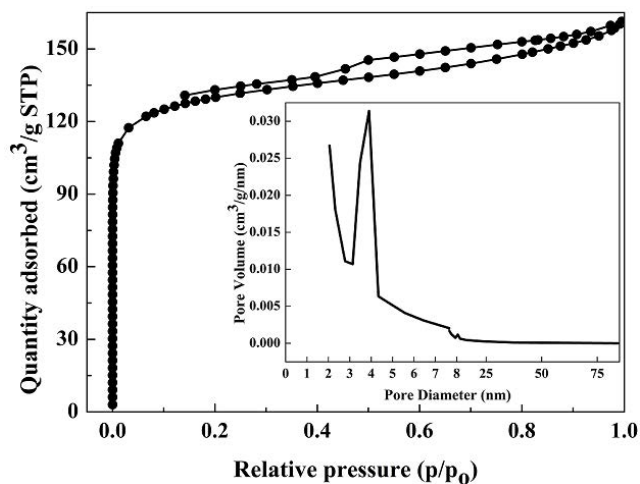


Fig. 3. N_2 adsorption–desorption isotherms of the TSMC and the pore size distribution based on the BJH method of the TSMC (inset).

Anyway, with the adding of the TSMC dosage, the equilibrium adsorption amounts always fell off, but the removal rates both went up observably and remain almost constant for phenol and 2,4-DCP. This phenomenon can be attributed to the explanation. The number of available adsorption sites increase with the increase in the TSMC dosage [27]. Therefore, it leads to the phenols removal rates increased rapidly. But the opposite trend in adsorption capacity is mainly attributed to the unsaturation of the adsorption sites through the adsorption process. The results of this unit also indicate that the appropriate TSMC dosage is extremely essential. In summary, the TSMC dosage is decided accurately at 0.2 g for phenol and 0.1 g for 2,4-DCP.

3.3. Effect of the solution pH

The variation in solution pH can influence the surface charge of the adsorbent materials and the ionization state of adsorbates, which consequently alters the adsorption capability. The effects of pH on the removal of phenol and

2,4-DCP were investigated in Fig. 5. In detail, the adsorption capabilities for phenol slowly reduce when the initial pH values ranges from 2.0 to 6.0, then vary only slightly, while it rapidly reduces in the region of $pH \geq 10.0$. And the similar situation occurs in adsorption of 2,4-DCP except the turning point being 7.0 for 2,4-DCP. The phenomenon can be explained by effect between surface property of the adsorbent and degree of ionization–dissociation of the adsorbate molecules [28].

At lower pH, both the TSMC surface and the phenols are in protonated form. In this case, no repulsion occurs between the TSMC surface and the phenols [6]. Besides, 2,4-DCP could be adsorbed onto the TSMC surface through the π - π interaction, which is attributed to the dispersion interaction between the electrons in the aromatic ring of 2,4-DCP and the surface of the TSMC while the π - π interaction between the phenolic ring and the TSMC basal planes is possible for phenol [1]. Moreover, the hydrogen bonding is also formed between phenol molecules and TSMC. And at alkaline pH, the surface of the TSMC is negatively charged. The electrical

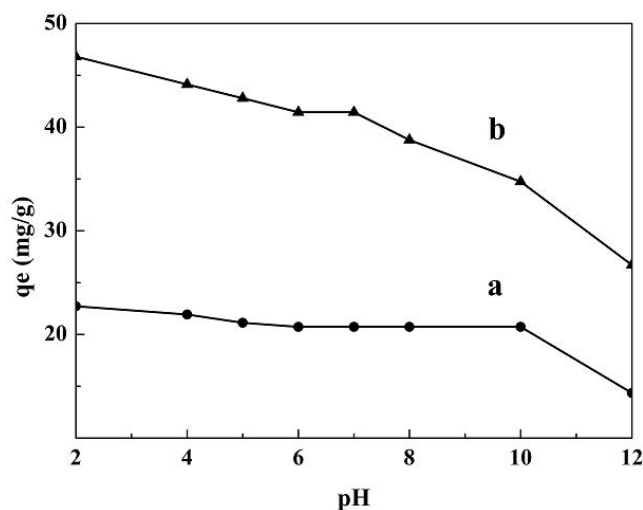


Fig. 5. Effect of the pH values on the adsorption of (a) phenol and (b) 2,4-DCP.

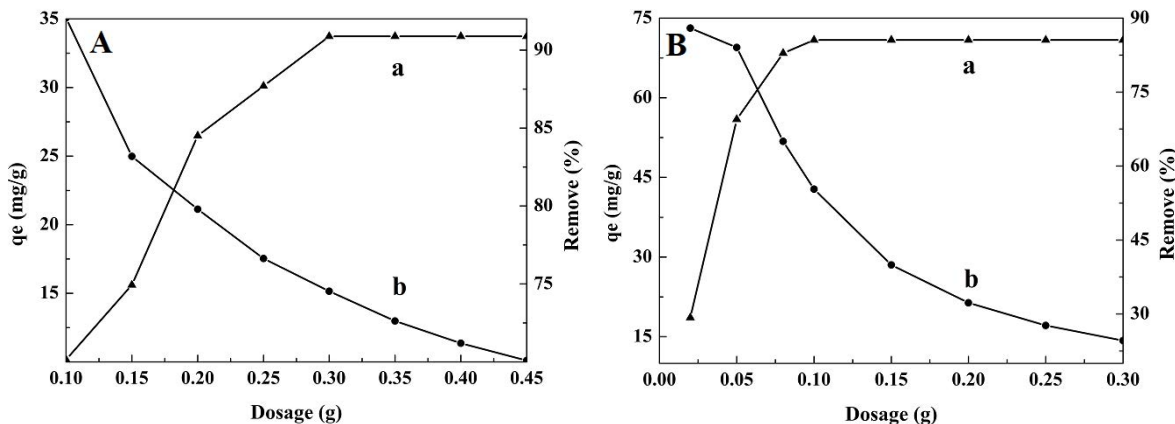


Fig. 4. Effect of the TSMC dosages on the adsorption of (A) phenol and (B) 2,4 DCP (a: removal rate (%), and b: adsorption capacity q_e [mg/g]).

repulsion between the identical charges lowers the adsorption capacities, which only occurs in the surface of the TSMC. However, it can be seen from Fig. 5, the adsorption capability decreases rapidly due to the repulsive force prevailing at higher pH (10.0 and 8.0 for phenol and 2,4-DCP, respectively), which may be explained by the pKa of phenols. Phenol and 2,4-DCP are weak acids (pKa values 9.89 and 7.90, respectively). With increasing the values of pH, phenol and 2,4-DCP are dissociated forming phenolate anions. Thus most of the phenol molecules and the TSMC are present in their negative ions, and it gives rise to the stronger electrostatic repulsion among the phenol anions and the negative charge on the surface of TSMC [20]. Besides, the dissociation of hydrogen ions has higher solubility in aqueous solution and form stronger adsorbate–water attractive interactions [29]. So the adsorption capability decreases sharply at a higher pH value.

3.4. Effect of the contact time

Contact time is an important parameter to determine the equilibrium time of adsorption process. The effect of contact time on the adsorption capacity of phenol and 2,4-DCP is shown in Fig. 6. For phenol, the first 15 min belongs to rapid adsorption, followed by a relatively slow increase, and reaches equilibrium in about 60 min. For 2,4-DCP, it is fast in the previous 30 min and then gradually slowing down, the adsorption is equilibrium until lasting 240 min. The elemental analysis shows that the TSMC is mainly composed of carbon (92.13%), with a small amount of hydrogen (2.43%). The phenol adsorption is related to the hydrogen bonding between the hydroxyl groups of phenol and the TSMC surface while the 2,4-DCP adsorption is related to the hydrogen bonding and the interaction between the hydroxyl groups and the choral groups of 2,4-DCP and the mesoporous carbon surface [30,31]. During a less-sharp rise portions, the adsorption capacity is retarded mainly by the formerly adsorbed molecules sited on the surface of the TSMC particles [2]. Eventually, the curves both reached a

plateau, indicating that the TSMC is saturated station with the equilibrated adsorption capacity of 21.92 mg/g (phenol) and 42.78 mg/g (2,4-DCP).

As shown in Fig. 6, the distinct differences in the adsorption capacity and the initial adsorption rate between phenol and 2,4-DCP are visible. Those occur because of the solubility of phenols. From Table 2, the solubility of phenol and 2,4-DCP are 93,000 and 4,500 mg/L, respectively. Phenol is the more hydrophilic in water than 2,4-DCP, thus the attraction from water molecules to phenol is the stronger than the 2,4-DCP, which could be attributed to the hydrogen bonding from water molecules to phenol [32].

3.5. Effect of the initial concentration

The effect of the initial concentration on the adsorption of phenol and 2,4-DCP by the TSMC was examined and the results are presented in Fig. 7. At the initial concentration from 20 to 160 mg/L, it is clear to see that the variation between the initial concentration and the equilibrium adsorption capacity may be viewed as a linear relationship. Similar behavior has been established by Sharma et al. [33] in which the simple adsorption of phenol on ground activated carbon was studied. In addition, the values of q_e rise more slowly with the initial concentration of 160–320 mg/L due to the mesoporous diffusivities. In detail, the phenols pore diffusion is reinforced and in the boundary layer is reduced, which leads to the pore diffusivities increasing [34]. Nevertheless, with the initial phenols concentration higher than 320 mg/L, there are no remarkable changes in q_e values. These may be the fact that the adsorption reaches saturation owing to the TSMC offering limited surface binding sites [35].

As shown in Fig. 7, it can be also found that 2,4-DCP demonstrates higher adsorption capacities than phenol with increasing the initial concentration. This different degree of adsorption may be explained in terms of the hydrophobic interactions. The *n*-octanol/water partition coefficient (K_{OW}) is an important hydrophobic parameter, which is the ratio of the

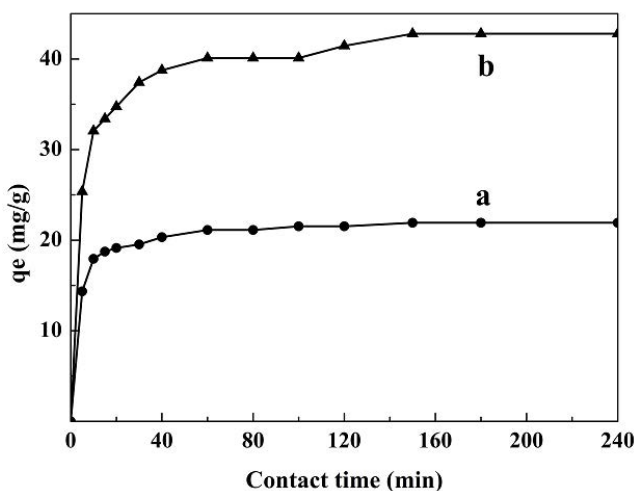


Fig. 6. Effect of the contact time on the adsorption of (a) phenol and (b) 2,4-DCP.

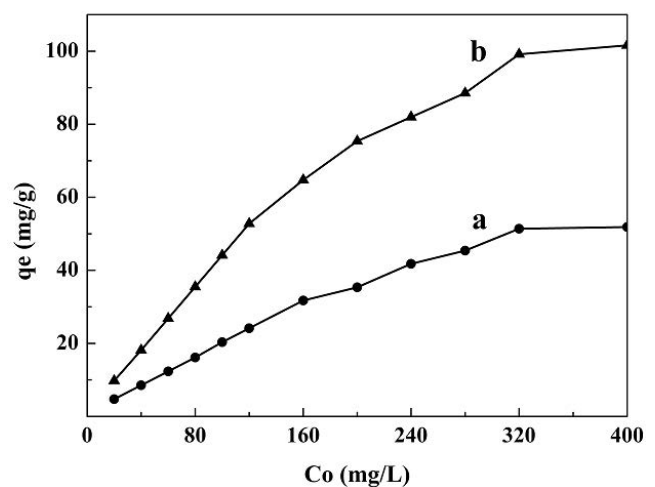


Fig. 7. Effect of the initial concentration on the adsorption of (a) phenol and (b) 2,4-DCP.

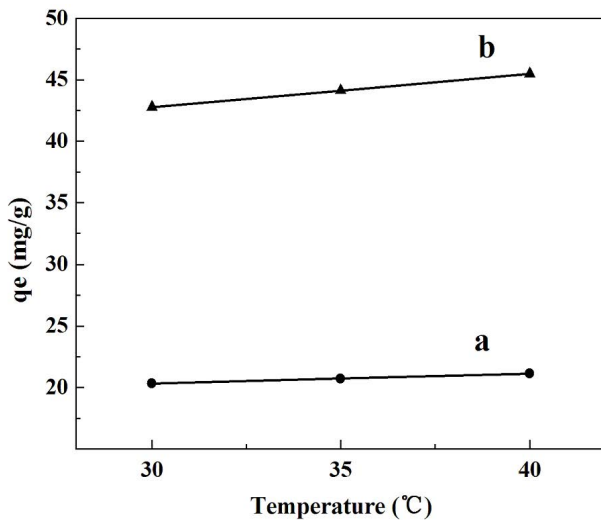


Fig. 8. Effect of the contact temperature on the adsorption of (a) phenol and (b) 2,4-DCP.

organic compounds concentration in *n*-octanol to that in water in a two-phase system at equilibrium [36]. The adsorption quantity of phenols increases with the development of the $\log K_{OW}$ values obtained from United States National Library of Medicine [37]. As suggested by Table 2, the values of $\log K_{OW}$ are 1.46 and 3.06 for phenol and 2,4-DCP, respectively. And the higher hydrophobic interactions exist in between the 2,4-DCP and the TSMC surface. Similar results are consistent with the observations of other authors' [21].

3.6. Effect of the contact temperature

The contact temperature is considered as a critical factor which may affect the adsorption process greatly. The effect of temperature on adsorption capability of the TSMC toward phenol and 2,4-DCP was examined by varying temperatures from 30°C to 40°C. The results are presented in Fig. 8. It is noteworthy that the adsorption capacity increases as the temperature rises. In detail, the adsorption capacity of phenol onto the TSMC is found to gradually increase from 20.33 to 21.13 mg/g with the temperature from 30°C to 40°C; and it also shows that the adsorption capacity of the TSMC toward 2,4-DCP demonstrates higher adsorption capacities from 42.78 to 45.47 mg/g by increasing the temperature, which all suggest that the adsorption processes are both endothermic in nature. The reason can be attributed to the fact that the high temperature can increase the rate of diffusion of the phenol molecules across the external boundary layer and in the internal surface of the TSMC [6]. Some researchers also describe this phenomenon on the basis of a swelling effect within which the internal structure of the TSMC enables phenols to penetrate further [7].

3.7. Studies of the adsorption equilibriums

3.7.1. Adsorption kinetics

Adsorption kinetics is one of the main indicators reflecting the adsorbent efficiency and providing information of

Table 3
Kinetic parameters for phenols adsorption onto the TSMC

Kinetic type	Kinetic parameters	Phenol	2,4-DCP
Pseudo-first-order	k_1 (1/min)	0.0223	0.0338
	q_e (mg/g)	5.5950	21.1198
	R^2	0.8720	0.8662
Pseudo-second-order	k_2 (g/mg/min)	0.01637	0.0054
	q_e (mg/g)	22.1680	43.3840
	R^2	0.9998	0.9992
Intraparticle diffusion	C (mg/g)	15.8420	27.0047
	k_3 (mg/g/min ^{1/2})	0.6890	1.7709
	R^2	0.9580	0.9371

the adsorption mechanism, which is an important characteristic to define the efficiency of adsorption. Therefore, in order to investigate the mechanism of adsorption and kinetic parameters were modeling by three nonlinear kinetic models including the pseudo-first order model [38], the pseudo-second order model [39] and the intraparticle diffusion model [40]. The pseudo-first-order model is given by the following equation:

$$\ln(q_e - q_t) = \ln q_e - k_1 t \quad (3)$$

where k_1 (1/min) is the pseudo-first-order rate constant, q_e (mg/g) is the adsorption capacity of the adsorbent at equilibrium, q_t (mg/g) is the adsorption capacity at time t .

Eq. (4) defines the pseudo-second-order model as follows:

$$\frac{t}{q_t} = \frac{1}{k_2 q_e^2} + \frac{1}{q_e} t \quad (4)$$

where k_2 (g/mg/min) is the pseudo-second-order rate constant, the modified parameter $k_2^* = k_2 q_e$ in the pseudo-second-order kinetic model is considered to be an adsorption rate constant, the rate constant $v_0 = k_2^* q_e^2$ in the pseudo-second-order kinetic model reflects the initial adsorption rate [41].

The fitted curves of phenol and 2,4-DCP are shown in Fig. 9 and the adsorption calculated kinetic parameters are listed in Table 3. It can be seen that the pseudo-first-order model gives poor fitting with low R^2 values (0.8720 and 0.8662 for phenol and 2,4-DCP, respectively) and significant differences between experimental and theoretical uptakes. However, the R^2 values obtained from the pseudo-second-order model are 0.9998 and 0.9992 for phenol and 2,4-DCP, respectively. Moreover, the calculated q_e values acquired from the pseudo-second-order model are in good agreement with the experimental data. Meanwhile, the modified parameter k_2^* is considered to be a more applicable rate constant to directly describe the adsorption kinetic process [42]. As calculated, the k_2^* values of phenol and 2,4-DCP are 0.3629 and 0.2343, respectively, indicating faster adsorption rate of phenol by the TSMC. Furthermore, the initial adsorption rate v_0 of phenol and 2,4-DCP is 7.8677 and 10.1649, respectively, which suggests that the initial adsorption rate of 2,4-DCP is also much faster than phenol. The results are in agreement with the observations from

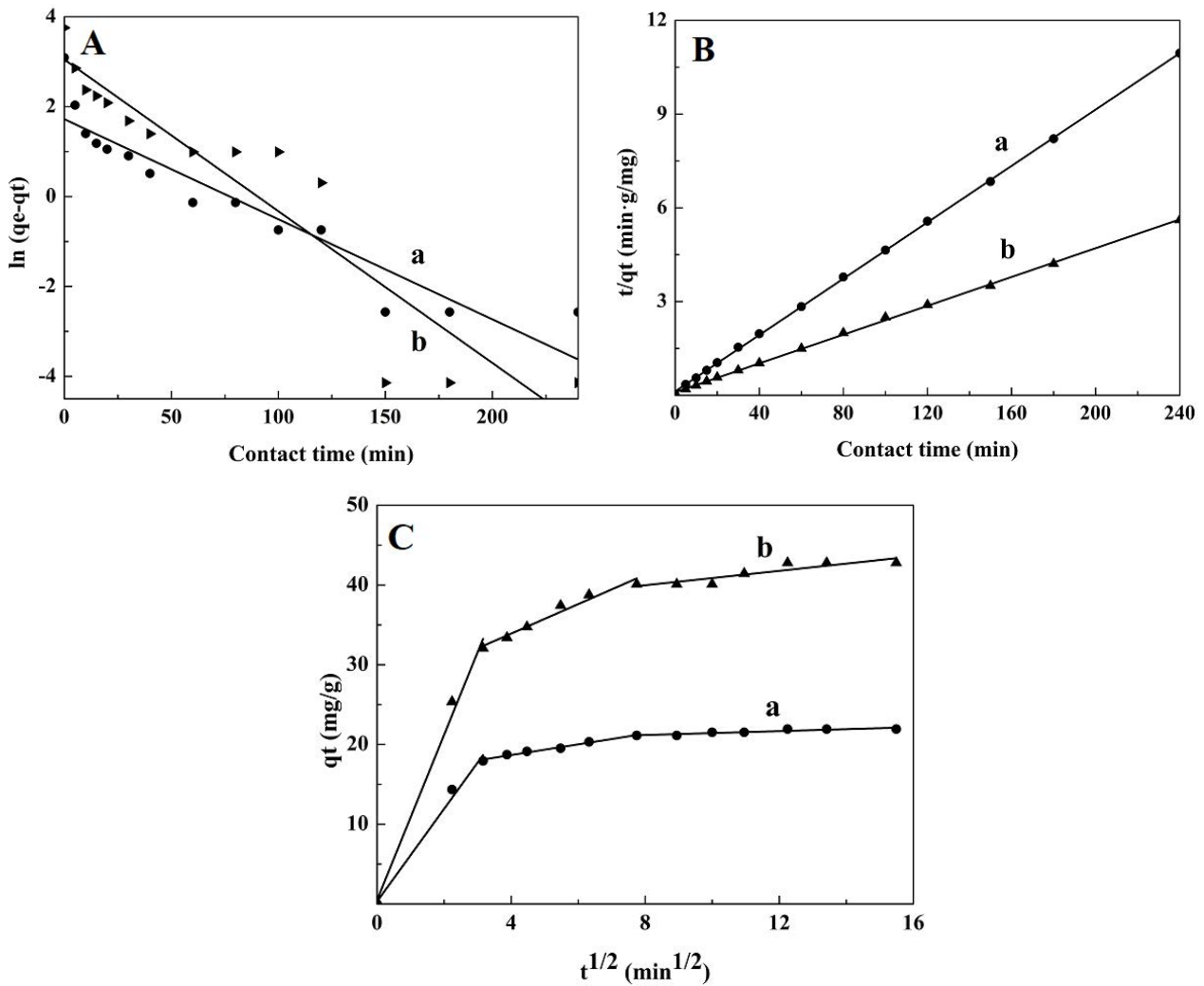


Fig. 9. Plots of the adsorption kinetics for (a) phenol and (b) 2,4-DCP; (A) the pseudo-first-order kinetics, (B) the pseudo-second-order and (C) the intraparticle diffusion.

Table 4
 Isotherm parameters for phenols adsorption onto the TSMC

Isotherm type	Isotherm parameters	Phenol	2,4-DCP
Langmuir	Q_m (mg/g)	62.0347	108.6957
	K_L (L/mg)	0.0284	0.0571
	R^2	0.9748	0.9912
	R_L	0.0809	0.0419
Freundlich	K_F	4.1095	13.5636
	n	1.9127	2.3941
	R^2	0.9675	0.9585
Dubinin–Radushkevich	q_m (mg/g)	27.2862	56.2182
	E (kJ/mol)	0.8273	1.4794
	R^2	0.4223	0.4497
Temkin	B_1 (J/mol)	10.9681	17.7163
	K_T	0.5041	1.3139
	R^2	0.8915	0.9282

Fig. 6. It demonstrates that the pseudo-second-order model rather than the pseudo-first-order model can be applied to the entire adsorption process.

The pseudo-first-order or pseudo-second-order kinetic models can provide information on adsorption capacity and adsorption rate, but they give no insight into the adsorption mechanism. So the intraparticle diffusion model is used to analyze and elucidate the diffusion mechanism. Generally, adsorption process on a mesoporous adsorbent may be controlled by three stages: external diffusion, intraparticle diffusion and adsorption onto sites. The intraparticle diffusion equation is expressed as follows:

$$q_t = k_3 t^{1/2} + C \quad (5)$$

where k_3 (g/mg/min^{1/2}) is the intraparticle diffusion rate constant, C (mg/g) is a constant related to the bounding layer thickness. If the plot passes through the origin ($C = 0$), then the intraparticle diffusion is the sole rate-limiting step. Otherwise, some other mechanism along with the intraparticle diffusion is also involved [43].

As can be seen from Fig. 9c, the phenol and 2,4-DCP exhibit multi-linear plots, suggesting that the adsorbent surface adsorption and the intraparticle diffusion are simultaneously occurring during the adsorption process and contribute to the adsorption mechanism. During the initial sharp rise stage, the diffusion of the phenols through the boundary layer to the external surface of the TSMC is restricted mainly by the mesoporous structure; during the following less-sharp rise stage, the intraparticle diffusion might be mainly related to the microporous diffusion [11]; and the plateau portion corresponds to the final equilibrium process due to extremely low concentration of phenols left in solution [44].

The calculated intraparticle diffusion parameters are listed in Table 3. The R^2 of phenol and 2,4-DCP for the intraparticle diffusion model are 0.9580 and 0.9371, respectively. Compared with phenol, the values of k_3 and C demonstrate a higher boundary layer effect and a higher diffusion rate constant for 2,4-DCP. These results indicate that the diffusion of phenol within the mesoporous structure of TSMC is more rapid than that of 2,4-DCP and the surface adsorption is the dominant step in the adsorption process [29].

3.7.2. Adsorption isotherms

As equilibrium adsorption isotherm is significantly important to the design of adsorption systems and can explain the adsorbate molecules distribution between the liquid phase and the solid phase when the adsorption process reaches an equilibrium state, in this study, the adsorption of phenol and 2,4-DCP onto TSMC was described mainly through Langmuir [45,46], Freundlich [46], D-R (Dubinin-Radushkevich) [47] and Temkin isotherm models [48].

The Langmuir isotherm is based on the assumption that there is a finite number of binding sites which are homogeneously over the adsorbent surface and a monolayer adsorption occurs without mutual interaction between the adsorbed molecules [49]. The linear form of the Langmuir isotherm equation can be represented by the following equation:

$$\frac{C_e}{q_e} = \frac{1}{Q_m K_L} + \frac{C_e}{Q_m} \quad (6)$$

where C_e (mg/L) is the equilibrium concentration of phenols in the liquid phase, q_e (mg/g) is the adsorption capacity of the adsorbent at equilibrium, Q_m (mg/g) is the maximum adsorption capacity corresponding to complete monolayer converge, and K_L (L/mg) is Langmuir constant related to the affinity of the binding sites. The essential characteristics of Langmuir isotherm can be expressed in terms of dimensionless equilibrium parameter or separation factor R_L , which is calculated by the following equation [50]:

$$R_L = \frac{1}{1 + K_L C_0} \quad (7)$$

where C_0 (mg/L) is the highest initial phenol concentration, the value of R_L indicates the type of the isotherm to be either unfavorable ($R_L > 1$), linear ($R_L = 1$), favorable ($0 < R_L < 1$) or irreversible ($R_L = 0$).

The Freundlich isotherm is an empirical model that is based on the adsorption on heterogeneous surfaces. In addition, it is supposed that the active sites with strong binding force are occupied by adsorbate primarily and then the adhesion decreased with the increase of site occupation [51]. The linearized Freundlich isotherm is represented by the following equation:

$$\ln q_e = \ln K_F + \frac{1}{n} \ln C_e \quad (8)$$

where K_F is the Freundlich constant related to the adsorption capacity, and n is the constant related to the adsorption intensity, which indicate the adsorption process to be either favorable ($1 < n < 10$) or poor ($n < 1$).

The D-R isotherm is more general than the Langmuir isotherm because it does not assume a homogeneous surface or constant adsorption potential, which has been extensively used to distinguish the physical and chemical adsorption [52]. The linear form of D-R isotherm equation is given as follows:

$$\ln q_e = \ln q_m - \beta \varepsilon^2 \quad (9)$$

$$\varepsilon = RT \ln \left(1 + \frac{1}{C_e} \right) \quad (10)$$

$$E = \frac{1}{\sqrt{2\beta}} \quad (11)$$

where q_m (mg/g) is the maximum adsorption capacity, β (mol²/kJ²) is the activity coefficient related to mean the adsorption energy contact, ε is the Polanyi potential, R (8.314 J/K/mol) is the universal gas constant, T (K) is the adsorptive Kelvin temperature and E (kJ/mol) is the mean free energy of adsorption.

The Temkin isotherm model describes that the heat of adsorption of all molecules in the layer would decrease with

the surface coverage. In addition, it assumes that the adsorption is characterized by a uniform distribution of the binding energies, up to some maximum binding energy [53]. The linear form of Temkin isotherm equation is as follows:

$$q_e = B_1 \ln K_T + B_1 \ln C_e \tag{12}$$

where K_T (mg/L) is the equilibrium binding constant corresponding to the maximum binding energy, $B_1 = RT/b$ (J/mol) is the Temkin constant related to heat of adsorption.

The fitting plots of the adsorption isotherms of phenol and 2,4-DCP onto the TSMC are shown in Fig. 10, and all the constants gained from the adsorption isotherm models are summarized in Table 4. According to the results listed in Table 4, the correlation coefficients values exceed 0.90 for the adsorption isotherm models except the D-R isotherm model, suggesting that the Langmuir, Freundlich and Temkin isotherm models closely fit the experimental results. At the same time, the Langmuir isotherm model (R^2 for phenol and 2,4-DCP are 0.9748 and 0.9912, respectively) is much more suitable than the Freundlich and Temkin isotherms for describing adsorption isotherm data. The fitness of the

Langmuir model to the adsorption process connotes that the phenol molecules from bulk solution were adsorbed on specific monolayer which is homogeneous in nature without mutual interaction between the adsorbed phenol molecules. Moreover, the R_L values (phenol and 2,4-DCP are 0.0809 and 0.0419, respectively) lie between 0 and 1, indicating a favorable behavior toward the adsorption of phenol and 2,4-DCP on the TSMC under the studied conditions.

With respect to the Freundlich isotherm model, the regression coefficients (R^2) for phenol and 2,4-DCP are 0.9675 and 0.9585, respectively, displaying that this model is not as good as the Langmuir isotherm model for describing the experimental data. It is observed that the values of n for phenol and 2,4-DCP are found 1.9147 and 1.3947, respectively, further indicating further that the adsorption processes tend to happen easily.

From Fig. 10C and Table 4, it can be observed that the worst fitting in all cases and the low regression coefficients for phenol and 2,4-DCP show that the D-R isotherm model could not interpret the data reasonably. The fitted curves of the Temkin isotherm model are depicted in Fig. 10D, and the calculated equilibrium data are listed in Table 4. The R^2

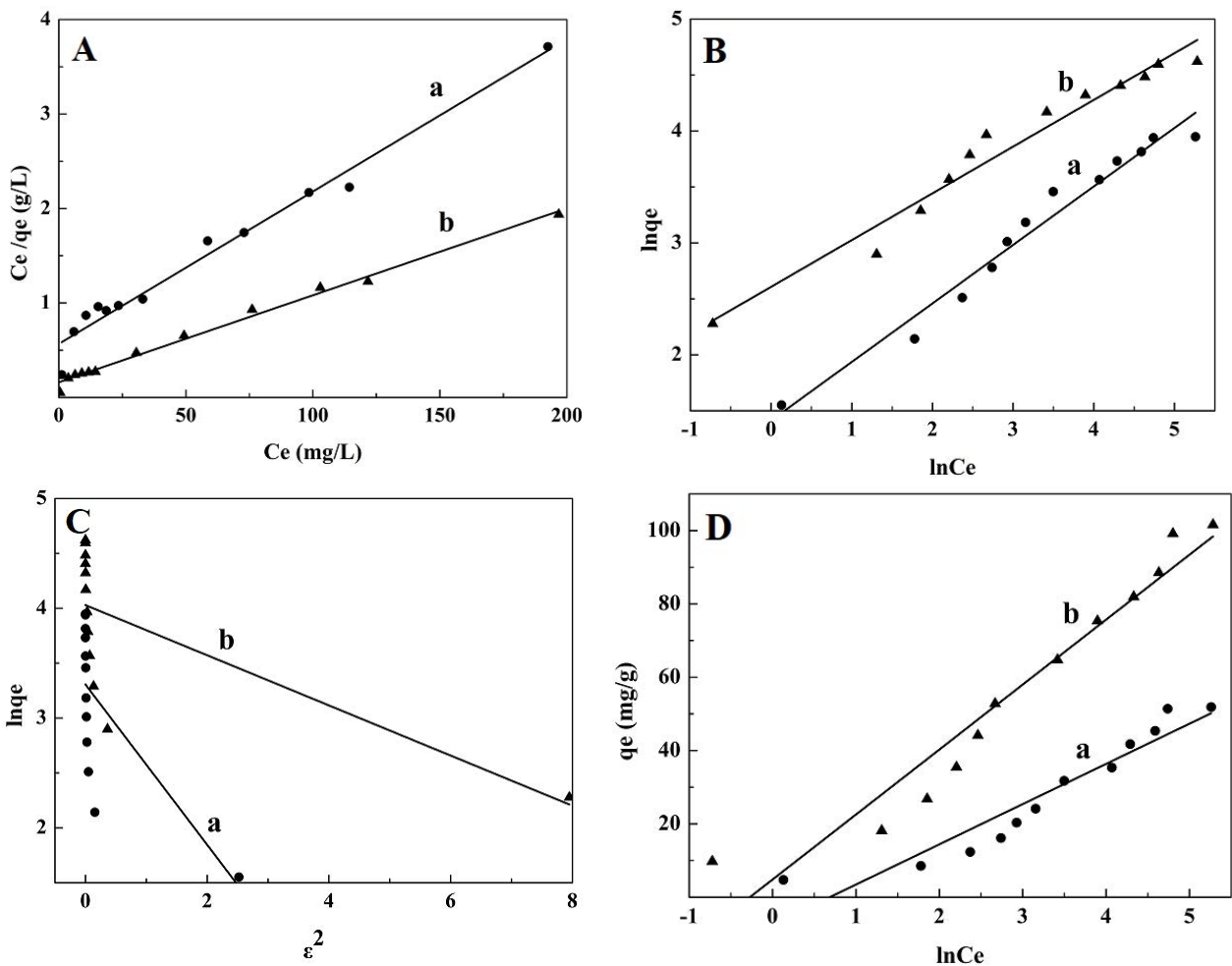


Fig. 10. Plots of the adsorption isotherms for (a) phenol and (b) 2,4-DCP; (A) Langmuir, (B) Freundlich, (C) Dubinin–Radushkevich and (D) Temkin isotherms.

values for phenol and 2,4-DCP are 0.8915 and 0.9282, respectively. It is possible to conclude that the 2,4-DCP adsorption on the TSMC can be described by the Temkin isotherm model, appropriately comparing with the experimental data.

In addition, the Langmuir isotherm model can provide information on maximum adsorption capacity. The maximum sorption capacities (Q_m) of phenol and 2,4-DCP are 62.0437 and 108.6957 mg/g, respectively, which are related to the relatively high surface area of the TSMC and its mesoporous structure [43]. Compared with the phenol, the 2,4-DCP exhibits the higher maximum adsorption capacity, which may be attributed to the chlorine substituents. On the one hand, increasing the number of chlorine substituents decrease its solubility significantly; on the other hand, as chlorine is an electron withdrawing group, an increase in chlorine substituents on an aromatic ring also decreases the electron density on the ring [54]. Thus 2,4-DCP possesses two more hydrophobic group and lower solubility as explained above, leading to 2,4-DCP being adsorbed more intensely than phenol.

3.7.3. Adsorption thermodynamics

In any adsorption process and engineering practice, the thermodynamic parameters such as change in standard Gibbs free energy (ΔG), enthalpy (ΔH) and entropy (ΔS) should be considered in order to determine whether the adsorption processes will occur spontaneously [55]. The relation between ΔG , ΔH and ΔS were calculated using the following equations reported in literatures [56]:

$$\Delta G = -RT \ln b \quad (13)$$

$$b = \frac{q_e}{C_e} \quad (14)$$

$$\Delta G = \Delta H - T\Delta S \quad (15)$$

$$\ln b = \frac{\Delta S}{R} - \frac{\Delta H}{RT} \quad (16)$$

where ΔG is the Gibbs free energy (kJ/mol), ΔH is the enthalpy (kJ/mol), ΔS is the entropy (J/mol/K), T (K) is the adsorptive Kelvin temperature, R (8.314 J/K/mol) is the universal gas constant, b is the partition coefficient.

The plots of the adsorption thermodynamics are shown in Fig. 11, and the parameters ΔG , ΔH and ΔS are listed in Table 5. The negative values of ΔG indicate spontaneous nature of the adsorption phenol and 2,4-DCP on TSMC. The decrease in values of ΔG with the increase in temperature indicates that the adsorption process is more favorable at higher temperature. Moreover, the value of ΔG for physical adsorption lies between -20 and 0 kJ/mol while the chemical adsorption ranges from -80 to -400 kJ/mol [57]. The values of ΔG (-0.2044 to -0.8024 kJ/mol and -2.8070 to -4.0443 kJ/mol for phenol and 2,4-DCP, respectively) also confirm phenol and 2,4-DCP were physical adsorption to the TSMC material, which is agreement with the above study.

As also can be seen from Table 5, the phenols adsorption onto TSMC give positive values of ΔH (17.924 and 34.7051 kJ/

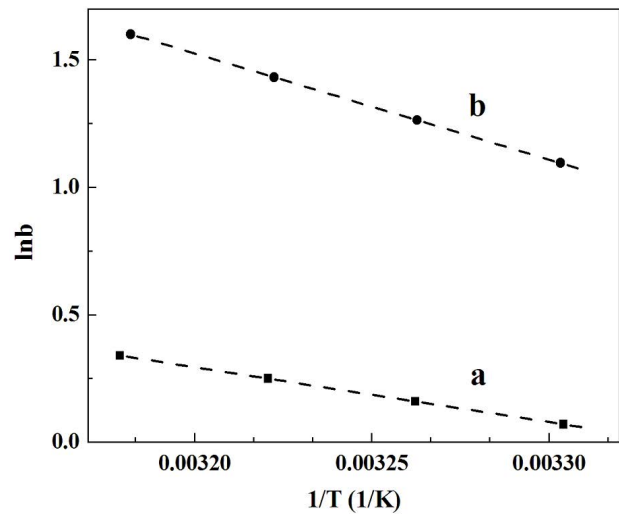


Fig. 11. Plots of the adsorption thermodynamics for (a) phenol and (b) 2,4-DCP.

Table 5
Thermodynamic parameters for phenols adsorption onto the TSMC

Parameters	Temperature	phenol	2,4-DCP
ΔG (kJ/mol)	303.15 (K)	-0.2044	-2.8070
	308.15 (K)	-0.5034	-3.4257
	313.15 (K)	-0.8024	-4.0444
ΔH (kJ/mol)		17.9240	34.7051
ΔS (J/mol/K)		59.8006	123.7407

mol for phenol and 2,4-DCP, respectively), indicating that both adsorption processes are endothermic in nature and favored in high temperature condition. Furthermore, the ΔH value of physical adsorption is less than 40 kJ/mol [58]. The positive values of ΔH demonstrate again that the adsorption of phenols on the TSMC is physical adsorption processes. And the values ΔS of phenol and 2,4-DCP are 59.8006 and 123.7407 J/mol/K, respectively, which signify that the adsorption processes are irreversible and have a good affinity for phenols toward the TSMC particles, together with having an increase in randomness at the solid-liquid interface during phenols displacing from the solution and fixating onto the active sites of TSMC [59].

4. Conclusions

In summary, the mesoporous carbon was successfully synthesized by the nanocasting method with sucrose as carbon source and KIT-6 as the structure-directing agent at 900°C. The obtained TSMC was characterized by XRD, TEM and N_2 adsorption-desorption techniques. And the results indicated that the obtained material possesses disordered worm-like mesoporous structure, uniform pore size distributions and high surface areas. And the obtained

TSMC exhibited a considerable performance toward phenol (21.126 mg/g) and 2,4-DCP (42.784 mg/g) under optimal conditions: the initial concentration of 100 mg/L; the contact temperature of 30°C; the TSMC dosages of 0.2 and 0.1 g, the initial pH values of 6.80 and 6.65, the adsorptions equilibriums times of 60 and 120 min, respectively. For the phenol and 2,4-DCP, both adsorption processes were fitted well with the pseudo-second-order kinetic model. Meanwhile, the equilibrium data were correlated better with the Langmuir isotherm model than other isotherm models. In addition, the thermodynamic constants including ΔG , ΔH and ΔS revealed that phenol and 2,4-DCP adsorption on the TSMC are both physical adsorption with the spontaneous, endothermic, and entropy-driven nature processes.

Acknowledgments

This work was supported by the Project for Importing Talent of Taiyuan University of Technology (tyut-rc201120a), the Scientific and Technological Innovation Programs of Higher Education Institutions in Shanxi (2015135), and the Shanxi Provincial Key Research and Development Plan (general) Social Development Project (201703D321009-5).

References

- [1] A. Sarswat, D. Mohan, Sustainable development of coconut shell activated carbon (CSAC) & magnetic coconut shell activated carbon (MCSAC) for phenol (2-nitrophenol) removal, *RSC Adv.*, 6 (2016) 85390–85410.
- [2] H. Ou, Q. You, J. Li, G. Liao, H. Xia, D. Wang, A rich-amine porous organic polymer: an efficient and recyclable adsorbent for removal of azo dye and chlorophenols, *RSC Adv.*, 6 (2016) 98487–98497.
- [3] X. Wu, Q. Zhang, C. Liu, X. Zhang, D.D.L. Chung, Carbon-coated sepiolite clay fibers with acid pre-treatment as low-cost organic adsorbents, *Carbon*, 123 (2017) 259–272.
- [4] L. Xu, Z. Wang, S. Ye, X. Sui, Removal of p-chlorophenol from aqueous solutions by carbon nanotube hybrid polymer adsorbents, *Chem. Eng. Res. Des.*, 123 (2017) 76–83.
- [5] H. Liu, R. Xia, D. Zhao, X. Fan, T. Feng, Enhanced adsorption of 2, 4-dichlorophenol by nanoscale zero-valent iron loaded on bentonite and modified with a cationic surfactant, *Ind. Eng. Chem. Res.*, 56 (2016) 1–10.
- [6] H. Yuan, Q.L. You, L.J. Song, Y.G. Liao, H. Xia, D.S. Wang, Preparation of carbon nanotubes/porous polyimide composites for effective adsorption of 2, 4-dichlorophenol, *RSC Adv.*, 6 (2016) 95825–95835.
- [7] F.W. Shaarani, B.H. Hameed, Ammonia-modified activated carbon for the adsorption of 2, 4-dichlorophenol, *Chem. Eng. J.*, 169 (2011) 180–185.
- [8] T.A. Saleh, S.O. Adio, M. Asif, H. Dafalla, Statistical analysis of phenols adsorption on diethylenetriamine-modified activated carbon, *J. Cleaner Prod.*, 182 (2018) 960–968.
- [9] P.T. Huong, B.K. Lee, J. Kim, Improved removal of 2-chlorophenol by a synthesized Cu-nano zeolite, *Process Saf. Environ.*, 100 (2016) 272–280.
- [10] W.P. Cheng, W. Gao, X.Y. Cui, J.H. Ma, R.F. Li, Phenol adsorption equilibrium and kinetics on zeolite X/activated carbon composite, *J. Taiwan Inst. Chem. Eng.*, 62 (2016) 192–198.
- [11] W. Libbrecht, A. Verberckmoes, J.W. Thybaut, D.V.P. Van, C.J. De, Tunable large pore mesoporous carbons for the enhanced adsorption of humic acid, *Langmuir*, 33 (2017) 6769–6777.
- [12] M.A. Islam, M.J. Ahmed, W.A. Khanday, M. Asif, B.H. Hameed, Mesoporous activated carbon prepared from NaOH activation of rattan (*Lacosperma secundiflorum*) hydrochar for methylene blue removal, *Ecotoxicol. Environ. Saf.*, 138 (2017) 279–285.
- [13] N. Katchala, J. Adduru, V. Upadhyayula, T.N. Rao, A. Srinivasan, Facile synthesis of mesoporous carbon from furfuryl alcohol-butanol system by EISA process for supercapacitors with enhanced rate capability, *J. Alloys Compd.*, 723 (2017) 488–497.
- [14] Y. Liu, X. Yang, H. Liu, Y. Ye, Z. Wei, Nitrogen-doped mesoporous carbon supported Pt nanoparticles as a highly efficient catalyst for decarboxylation of saturated and unsaturated fatty acids to alkanes, *Appl. Catal., B*, 218 (2017) 679–689.
- [15] T.Y. Ma, L. Liu, Z.Y. Yuan, Direct synthesis of ordered mesoporous carbons, *Chem. Soc. Rev.*, 42 (2013) 3977–4003.
- [16] W. Xin, Y. Song, Mesoporous carbons: recent advances in synthesis and typical applications, *RSC Adv.*, 5 (2015) 83239–83285.
- [17] H. Najafinezhad, Fabrication of magnetic mesoporous carbon and its application for adsorptive removal of 2, 4, 6-trichlorophenol (TCP) from aqueous solution, *Crystengcomm*, 16 (2014) 5598–5607.
- [18] J. Gao, X. Wang, Q. Zhao, Y. Zhang, J. Liu, Synthesis and supercapacitive performance of three-dimensional cubic-ordered mesoporous carbons, *Electrochim. Acta*, 163 (2015) 223–231.
- [19] J. Fan, X. Ran, Y. Ren, C. Wang, J. Yang, W. Teng, Ordered mesoporous carbonaceous materials with tunable surface property for enrichment of hexachlorobenzene, *Langmuir*, 32 (2016) 9922–9929.
- [20] S. Xue, C. Wang, Y. Wei, Preparation of magnetic mesoporous carbon from polystyrene-grafted magnetic nanoparticles for rapid extraction of chlorophenols from water samples, *RSC Adv.*, 7 (2017) 11921–11928.
- [21] M. Kragulj, J. Trickovic, A. Kukovec, B. Jović, J. Molnar, S. Rončević, Adsorption of chlorinated phenols on multiwalled carbon nanotubes, *RSC Adv.*, 5 (2015) 24920–24929.
- [22] Z. Luo, M. Gao, S. Yang, Q. Yang, Adsorption of phenols on reduced-charge montmorillonites modified by bispyridinium dibromides: mechanism, kinetics and thermodynamics studies, *Colloids Surf., A*, 482 (2015) 222–230.
- [23] J. Cao, C.J. Jafta, G. Jiang, Q. Ran, X. Lin, R. Félix, Synthesis of dispersible mesoporous nitrogen-doped hollow carbon nanoplates with uniform hexagonal morphologies for supercapacitors, *ACS Appl. Mater. Interfaces*, 8 (2016) 29628–29636.
- [24] G. Wang, S. Chen, X. Quan, H. Yu, Y. Zhang, Enhanced activation of peroxymonosulfate by nitrogen doped porous carbon for effective removal of organic pollutants, *Carbon*, 115 (2017) 730–739.
- [25] N. Moreno, A. Caballero, L. Hernán, J. Morales, J. Canales-Vázquez, Ordered mesoporous carbons obtained by a simple soft template method as sulfur immobilizers for lithium-sulfur cells, *Phys. Chem. Chem. Phys.*, 16 (2014) 17332–17340.
- [26] X. Yang, J. Yu, W. Zhang, G. Zhang, Mesopore-dominant wormhole-like carbon with high supercapacitive performance in organic electrolyte, *RSC Adv.*, 7 (2017) 15096–15101.
- [27] Y. Zhu, P. Kolar, Investigation of adsorption of p-cresol on coconut shell-derived activated carbon, *J. Taiwan Inst. Chem. Eng.*, 68 (2016) 138–146.
- [28] L. Jiang, L. Lu, S. Xiao, J. Chen, Preparation of a novel manganese oxide-modified diatomite and its aniline removal mechanism from solution, *Chem. Eng. J.*, 284 (2016) 609–619.
- [29] R. Liang, J. Zhang, Y. Li, C. Zhang, Preparation and evaluation of cattail fiber-based activated carbon for 2, 4-dichlorophenol and 2, 4, 6-trichlorophenol removal, *Chem. Eng. J.*, 168 (2011) 553–561.
- [30] A. Chen, Y. Li, Y. Yu, Y. Li, L. Zhang, H. Lv, Mesoporous carbonaceous materials prepared from used cigarette filters for efficient phenol adsorption and CO₂ capture, *RSC Adv.*, 5 (2015) 107299–107306.
- [31] Q.S. Liu, T. Zheng, P. Wang, J.P. Jiang, N. Li, Adsorption isotherm, kinetic and mechanism studies of some substituted phenols on activated carbon fibers, *Chem. Eng. J.*, 157 (2010) 348–356.
- [32] H. Ding, X. Shen, C. Chen, X. Zhang, Molecular dynamics simulations of simple aromatic compounds adsorption on single-walled carbon nanotubes, *RSC Adv.*, 6 (2016) 80972–80980.
- [33] M. Sharma, R.K. Vyas, K. Singh, Theoretical and experimental analysis of reactive adsorption in a packed bed: parallel and

- branched pore-diffusion model approach, *Ind. Eng. Chem. Res.*, 55 (2016) 5945–5954.
- [34] S. Varghese, V.P. Vinod, T.S. Anirudhan, Kinetic and equilibrium characterization of phenols adsorption onto a novel activated carbon in water treatment, *Indian J. Chem. Technol.*, 11 (2004) 825–833.
- [35] K.L. Lin, J.Y. Pan, Y.W. Chen, R.M. Cheng, X.C. Xu, Study the adsorption of phenol from aqueous solution on hydroxyapatite nanopowders, *J. Hazard. Mater.*, 161 (2009) 231–240.
- [36] A. Breindl, B. Beck, T. Clark, R.C. Glen, Prediction of then-octanol/water partition coefficient, logP, using a combination of semiempirical MO-calculations and a neural network, *Mol. Model. Annu.*, 3 (1997) 142–155.
- [37] J. Yang, G. Krishnamoorthy, A. Saxena, G. Zhang, J. Shi, H. Yang, Adsorption of phenols by magnetic polysulfone microcapsules containing tributyl phosphate, *Chem. Eng. J.*, 157 (2010) 466–474.
- [38] K. Anzo, M. Harada, T. Okada, Enhanced kinetics of pseudo first-order hydrolysis in liquid phase coexistent with ice, *J. Phys. Chem. A*, 117 (2013) 10619–10625.
- [39] Y.S. Ho, G. McKay, Pseudo-second order model for sorption processes, *Process Biochem.*, 34 (1999) 451–465.
- [40] W.J. Weber, J.C. Morris, Kinetics of adsorption on carbon from solution, *J. Sanit. Eng. Div.*, 1 (1963) 1–2.
- [41] Y. Dai, J. Yao, Y. Song, S. Wang, Y. Yuan, Enhanced adsorption and degradation of phenolic pollutants in water by carbon nanotube modified laccase-carrying electrospun fibrous membranes, *Environ. Sci. Nano.*, 3 (2016) 857–868.
- [42] P. Bo, B. Xing, Adsorption kinetics of 17 α -ethinyl estradiol and bisphenol A on carbon nanomaterials. I. Several concerns regarding pseudo-first order and pseudo-second order models, *J. Soils Sediments*, 10 (2010) 838–844.
- [43] Z.N. Garba, A.A. Rahim, Evaluation of optimal activated carbon from an agricultural waste for the removal of para-chlorophenol and 2,4-dichlorophenol, *Process Saf. Environ. Prot.*, 102 (2016) 54–63.
- [44] J. Pan, X. Zou, X. Wang, G. Wei, Y. Yan, J. Han, Selective recognition of 2,4-dichlorophenol from aqueous solution by uniformly sized molecularly imprinted microspheres with β -cyclodextrin/attapulgitic composites as support, *Chem. Eng. J.*, 162 (2010) 910–918.
- [45] I. Langmuir, The constitution and fundamental properties of solids and liquids, *J. Franklin Inst.*, 184 (1916) 102–105.
- [46] K.Y. Foo, B.H. Hameed, Insights into the modeling of adsorption isotherm systems, *Chem. Eng. J.*, 156 (2010) 2–10.
- [47] M.M. Dubinin, L.V. Radushkevich, Equation of the Characteristic Curve of Activated Charcoal, *Proceedings of the Union of Soviet Socialist Republics Academy of Sciences*, 55 (1947) 331–337.
- [48] C. Aharoni, M. Ungarish, Kinetics of activated chemisorption. Part 2. Theoretical models, *J. Chem. Soc., Faraday Trans.*, 73 (1977) 456–464.
- [49] E. Conde, A. Moure, H. Domínguez, Recovery of phenols from autohydrolysis liquors of barley husks: kinetic and equilibrium studies, *Ind. Crop. Prod.*, 103 (2017) 175–184.
- [50] H. Tahermansouri, Z. Dehghan, F. Kiani, Phenol adsorption from aqueous solutions by functionalized multiwalled carbon nanotubes with pyrazoline derivative in the presence of ultrasound, *RSC Adv.*, 5 (2015) 44263–44273.
- [51] J. Zhou, B. Yang, Z. Li, L. Lei, X. Zhang, Selective adsorption of naphthalene in aqueous solution on mesoporous carbon functionalized by task-specific ionic liquid, *Ind. Eng. Chem. Res.*, 54 (2015) 2329–2338.
- [52] V.S. Munagapati, V. Yarramuthi, D.S. Kim, Methyl orange removal from aqueous solution using goethite, chitosan beads and goethite impregnated with chitosan beads, *J. Mol. Liq.*, 240 (2017) 329–339.
- [53] M. Saad, H. Tahir, D. Ali, Green synthesis of Ag-Cr-AC nanocomposites by *Azadirachta indica* and its application for the simultaneous removal of binary mixture of dyes by ultrasonicated assisted adsorption process using response surface methodology, *Ultrason. Sonochem.*, 38 (2017) 197–213.
- [54] Q. Qin, K. Liu, D. Fu, H. Gao, Effect of chlorine content of chlorophenols on their adsorption by mesoporous SBA-15, *J. Environ. Sci.*, 24 (2012) 1411–1417.
- [55] R.I. Yousef, B. El-Eswed, A.A.H. Al-Muhtaseb, Adsorption characteristics of natural zeolites as solid adsorbents for phenol removal from aqueous solutions: kinetics, mechanism and thermodynamics studies, *Chem. Eng. J.*, 171 (2011) 1143–1149.
- [56] M. Kilic, E. Apaydinvarol, A.E. Pütün, Adsorptive removal of phenol from aqueous solutions on activated carbon prepared from tobacco residues: equilibrium, kinetics and thermodynamics, *J. Hazard. Mater.*, 189 (2011) 397–403.
- [57] L. Jiang, S. Li, H. Yu, Z. Zou, X. Hou, F. Shen, Amino and thiol modified magnetic multi-walled carbon nanotubes for the simultaneous removal of lead, zinc, and phenol from aqueous solutions, *Appl. Surf. Sci.*, 369 (2016) 398–413.
- [58] Y. Liu, J. Chen, M. Chen, B. Zhang, D. Wu, Q. Cheng, Adsorption characteristics and mechanism of sewage sludge-derived adsorbent for removing sulfonated methyl phenol resin in wastewater, *RSC Adv.*, 5 (2015) 76160–76169.
- [59] P.S. Thue, M.A. Adebayo, E.C. Lima, J.M. Sieliechi, F.M. Machado, G.L. Dotto, Preparation, characterization and application of microwave-assisted activated carbons from wood chips for removal of phenol from aqueous solution, *J. Mol. Liq.*, 223 (2016) 1067–1080.